

# Supplementary information for: “Non-Fermi-liquid behavior in metallic quasicrystals with local magnetic moments”

Eric C. Andrade,<sup>1</sup> Anuradha Jagannathan,<sup>2</sup> Eduardo Miranda,<sup>3</sup> Matthias Vojta,<sup>4</sup> and Vladimir Dobrosavljević<sup>5</sup>

<sup>1</sup>*Instituto de Física Teórica, Universidade Estadual Paulista,*

*Rua Dr. Bento Teobaldo Ferraz, 271 - Bl. II, 01140-070, São Paulo, SP, Brazil*

<sup>2</sup>*Laboratoire de Physique des Solides, CNRS-UMR 8502, Université Paris-Sud, 91405 Orsay, France*

<sup>3</sup>*Instituto de Física Gleb Wataghin, Unicamp, Rua Sérgio Buarque de Holanda, 777, CEP 13083-859 Campinas, SP, Brazil*

<sup>4</sup>*Institut für Theoretische Physik, Technische Universität Dresden, 01062 Dresden, Germany*

<sup>5</sup>*Department of Physics and National High Magnetic Field Laboratory, Florida State University, Tallahassee, FL 32306*

(Dated: June 3, 2015)

## I. ELECTRONIC WAVEFUNCTIONS IN THE OCTAGONAL TILING

Based on the results for one-dimensional quasicrystals,<sup>1</sup> we expect the resulting wavefunctions in quasiperiodic tight-binding models to be different both from the exponentially localized wavefunctions found in Anderson insulators as well from Bloch states found in a crystal. Such wavefunctions are the so-called *critical* wavefunctions. In real space, this means very large fluctuations of the wavefunction amplitude from site to site but with similar amplitudes on sites of similar local environment (the amplitude distribution is thus determined by the deterministic scale invariant geometry).

To probe the real space profile of the wavefunctions, we compute the inverse participation ratio

$$P_\nu^{-1} = \sum_i |\psi_\nu^c(i)|^4, \quad (\text{S1})$$

where  $\psi_\nu^c$  is an eigenstate of  $\mathcal{H}_c$  (defined in Eq. [1] of the main text) with energy  $E_\nu^c$ . The scaling of  $P_\nu^{-1}$  with the system size is related to the spatial structure of the electronic states. If we write  $P_\nu^{-1} \propto N_a^{-\beta}$ , then  $\beta = 1$  for extended and  $\beta = 0$  for exponentially localized states. In a quasicrystal, because of the critical nature of the wavefunctions, we expect that  $0 \leq \beta \leq 1$ . It is important to point out that the converse it is not true. For instance,  $\beta \approx 1$  does not necessarily imply an extended state. To establish such result, we need to study the scaling of the higher moments of the wavefunction distribution because the exponents that describe the scaling of these moments with  $N_a$  are not just multiples of each other – a property of multifractality.<sup>2-4</sup> As mentioned above, this resulting multifractal character of wavefunctions is a consequence of the invariance of quasicrystals under scale transformations, a feature called inflation-deflation symmetry.<sup>5</sup>

In Fig. S1 we calculate  $P_\nu^{-1}$  at different positions in the band (but away from the band center) and obtain  $\beta \approx 0.90$ , which is close but smaller than one and consistent with a preponderance of multifractal eigenstates. Remarkably, this is similar to the value of  $\beta$  reported for the Penrose tiling.<sup>6</sup>

Another useful quantity that probes the nature of the

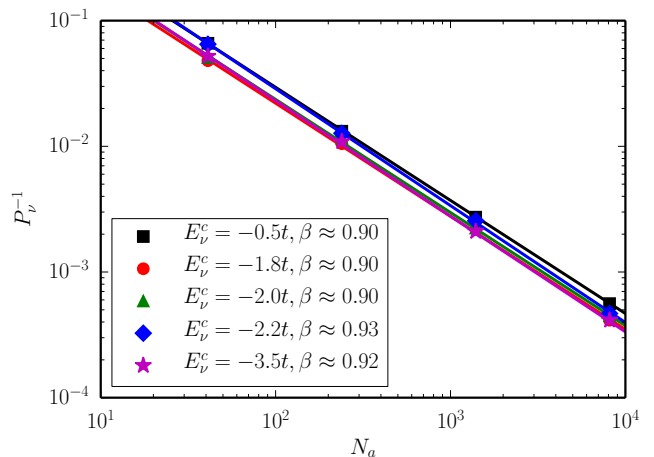


Figure S1: Octagonal tiling. Inverse participation ratio  $P_\nu^{-1}$  as a function of the approximant size  $N_a$  for different values of the eigenenergies  $E_\nu^c$  on a log-log scale. We considered four approximant sizes  $N_a = 41, 239, 1393, 8119$ . The solid lines are power-law fits:  $P_\nu^{-1} \propto N_a^{-\beta}$ .

wavefunction is the local density of states (LDOS)

$$\rho_i^c(\omega) = \overline{\sum_\nu |\psi_\nu^c(i)|^2 \delta(\omega - E_\nu^c)}, \quad (\text{S2})$$

where the overline denotes average over boundary conditions. The distribution of the logarithm of  $\rho_i^c(\omega)$  is presented in Fig. S2. As we can see, the curves are all qualitatively the same, indicating that the spatial fluctuations of  $\rho_i^c$  are, to a good extent, energy-independent and well described by a log-normal distribution (see the inset). Specifically, the width of the distribution does not vary much with the energy, except for  $\omega = -2.0t$  where there is a slightly larger tendency to have  $\rho_i^c(\omega)$  smaller than its typical value.

Generally, a log-normal distribution of LDOS is expected to occur in an Anderson insulator,<sup>7</sup> but it is also known that a log-normal also nicely describes the distribution of LDOS of disordered metals.<sup>8</sup> Therefore, a careful finite-size scaling study is required to establish the precise nature of the wavefunction based on  $P(\rho)$ .<sup>8</sup> We leave this more detailed investigation for a future work.

To conclude the discussion on the octagonal tiling,

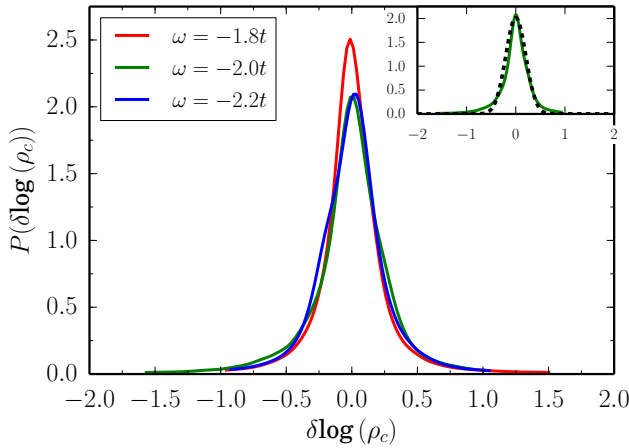


Figure S2: Octagonal tiling. Distribution of  $\delta \log(\rho_c) = \log(\rho_c) - \langle \log(\rho_c) \rangle$  at three different values of the energy  $\omega$ . Inset: The full curve correspond to  $P(\delta \log(\rho_c))$  at  $\omega = -2.0t$  and the dashed curve is a Gaussian fit to it. Here we considered the  $N_a = 8119$  approximant with  $N_\phi = 64$ .

we briefly mention our implementation of averaging over twisted boundary conditions (TBC).<sup>9,10</sup> This step was instrumental in obtaining reliable results since it provides a controlled way to eliminate finite-size effects associated with spectral discreteness (we will come back to the role of finite-size effects later). The average over TBC is completely equivalent to a periodic repetition of the  $N_a$ -site approximant in both directions using  $N_\phi$  copies, hence the effective total linear system size is increased to  $\sqrt{N_a N_\phi}$ .

## II. SLAVE BOSONS MEAN-FIELD EQUATIONS AND THE KONDO LIMIT

Minimizing the slave boson (SB) mean-field free energy, Eq. [2] in the main text, with respect to  $\tilde{\varepsilon}_\ell$  and  $Z_\ell$  we obtain the corresponding self-consistency equations

$$\frac{2}{\pi} \int_{-\infty}^{+\infty} f(\omega) \text{Im} \left[ \tilde{G}_\ell^f(\omega) \right] d\omega + Z_\ell - 1 = 0, \quad (\text{S3})$$

$$\frac{2}{\pi} \int_{-\infty}^{+\infty} f(\omega) \text{Im} \left[ \tilde{G}_\ell^f(\omega) \Delta_{f\ell}(\omega) \right] d\omega + \tilde{\varepsilon}_{f\ell} - E_f = 0. \quad (\text{S4})$$

In general, we solve these mean-field equations numerically at  $T = 0$ . They are algebraic non-linear equations on the parameters  $Z_\ell$  and  $\tilde{\varepsilon}_{f\ell}$ , which we solve using a globally convergent implementation of the Newton-Raphson algorithm.<sup>11</sup> The integral over frequencies is performed using the Romberg method.<sup>11</sup>

If we now move to the Kondo limit, where both  $Z_\ell, \tilde{\varepsilon}_{f\ell} \rightarrow 0$ , we are able to solve Eqs. (S3) and (S4) analytically. In this limit, we ignore the frequency dependence of the hybridization function,  $\Delta_{f\ell}(\omega) \simeq \Delta'_{f\ell}(0) +$

$i\Delta''_{f\ell}(0)$ , and assume that the integrals are dominated by their values at the Fermi level. From Eq. (S3) we obtain

$$\tilde{\varepsilon}_f + Z_\ell \Delta'_{f\ell}(0) \simeq 0. \quad (\text{S5})$$

which reflects the well-known fact that in the Kondo limit the position of the Kondo peak,  $\tilde{\varepsilon}_f + Z_\ell \Delta'_{f\ell}(0)$ , moves to the Fermi level.

From Eq. (S4) we can now calculate the Kondo temperature (recall our definition  $T_K^\ell \equiv Z_\ell \Delta''_{f\ell}(0)$ )

$$T_K^\ell = D \exp \left[ -\frac{\pi}{2} \frac{\Delta'_{f\ell}(0) + |E_f|}{\Delta''_{f\ell}(0)} \right], \quad (\text{S6})$$

where  $D$  is a high-energy cutoff of the integral of the order of the bandwidth. We recover the usual Kondo expression,  $T_K^\ell = D \exp[-1/J\rho_\ell^c(0)]$ , in the case of particle-hole symmetry,  $\Delta'_{f\ell}(0) = 0$ , with  $\Delta''_{f\ell}(0) = \pi V^2 \rho_\ell^c(0)$  and  $J = 2V^2/|E_f|$ .

## III. ASYMPTOTIC EXPRESSION FOR $P(T_K)$

Each site of the tiling has a different local  $c$ -electron cavity function  $\Delta_{c\ell}(\omega)$ , reflecting the fact that the effective potential that one electron sees as it goes through the lattice changes from site to site. If we go one step further, we may consider its real part at the Fermi level,  $\Delta'_{c\ell}(0)$ , as a renormalized on-site site energy for the  $c$ -electrons. According to the arguments presented in Ref. 12 for the case of weakly disordered Kondo systems, a power-law distribution for the Kondo temperature can be easily obtained provided that the fluctuations of  $\Delta'_{c\ell}(0)$ ,  $\delta\Delta'_c \equiv \Delta'_c(0) - \langle \Delta'_c(0) \rangle$ , follow a Gaussian distribution (see the inset of Fig. 3 of the main text). In disordered systems, the fluctuations of the local  $c$ -electron cavity function at a given site  $i$  result from Friedel oscillations of the electronic wavefunctions induced by other impurities which may lie at a relatively long distance from  $i$ . Furthermore, at weak disorder,  $\delta\Delta'_{c\ell}$  takes the form of a linear superposition of contributions from single impurity scatterers, and thus of a sum of independent random numbers, for which we expect the central limit theorem to hold. From our numerical results, we then reason that a similar mechanism takes place in quasicrystals. This somewhat surprising resemblance between a quasicrystal and weakly disordered systems, rather than systems at the metal-insulator transition, is also present in different physical quantities, e.g. the level-spacing distribution.<sup>5,6,13</sup> It indicates that a quasicrystal in higher dimensions may show a more conventional behavior in local quantities despite its multifractal eigenstates.

It is now a straightforward exercise to obtain the asymptotic expression  $P(T_K) \sim T_K^{\alpha-1}$  following Ref. 12. We start by relating the  $f$ -level hybridization function  $\Delta_{f\ell}$  with the local  $c$ -electron cavity function  $\Delta_{c\ell}$  at the

impurity site  $\ell$

$$\Delta'_{f\ell}(\omega) = \frac{V^2(\omega - \Delta'_{c\ell}(\omega))}{(\omega - \Delta'_{c\ell}(\omega))^2 + (\Delta''_{c\ell}(\omega))^2}, \quad (\text{S7})$$

$$\Delta''_{f\ell}(\omega) = \frac{V^2\Delta''_{c\ell}(\omega)}{(\omega - \Delta'_{c\ell}(\omega))^2 + (\Delta''_{c\ell}(\omega))^2}, \quad (\text{S8})$$

where, as usual, single (double) primes denote the real (imaginary) part. The next step is to take the Kondo limit making use of Eq. (S6). As the last assumption, we disregard fluctuation in the imaginary part of  $\Delta_{c\ell}(0)$ , so we replace  $\Delta''_{c\ell}(0)$  by its average value  $\langle\Delta''_c(0)\rangle$ . Using Eqs. (S7) and (S8) we then obtain

$$T_K^\ell = T_K^0 \exp\left[-\pi \frac{(\Delta'_{c\ell}(0))^2}{J\langle\Delta''_c(0)\rangle}\right], \quad (\text{S9})$$

where  $T_K^0 \equiv D \exp[-\pi\langle\Delta''_c(0)\rangle/J]$ . Inverting Eq. (S9) we may write

$$\delta\Delta'_{c\ell} \simeq \ln^{1/2}\left[\frac{T_K^0}{T_K^\ell}\right]^\lambda, \quad (\text{S10})$$

with  $\lambda = J\langle\Delta''_c(0)\rangle/\pi$  and we also considered the fact that for  $T_K^\ell \ll T_K^0$  we may drop the term  $\langle\Delta'_{c\ell}(0)\rangle$ . Since we assume that  $P(\delta\Delta'_c)$  is a simple Gaussian with variance  $\sigma_c$ , a direct change of variables gives, up to a negligible logarithmic correction,

$$P(T_K) \propto T_K^{\alpha-1}, \quad (\text{S11})$$

with

$$\alpha = \frac{J\langle\Delta''_c(0)\rangle}{2\pi\sigma_c^2} \sim J\langle\rho_c(0)\rangle. \quad (\text{S12})$$

So we see that  $\alpha$  varies linearly with  $J$  with a slope proportional to  $\langle\rho_c(0)\rangle$ .

To check the plausibility of our assumptions, we produced a scatter plot of the numerically calculated  $T_K^\ell$  versus the exponent of the Kondo limit formulas for  $T_K^\ell$  in Eqs. (S6) and (S9), Fig. S3. There, we see that all the points (one for each site in the quasicrystal approximant) follow a straight line, specially as  $T_K^\ell$  decreases, clearly indicating a strong correlation between the full numerics and the asymptotic expressions for the  $T_K^\ell$ . Additional scatter around this straight line simply reflects departures from Eqs. (S6) and (S9), i.e. a situation where the value  $T_K^\ell$  depends not only on  $\Delta_{f\ell}$  at the Fermi level, but on the entire spectral function. Moreover, as  $T_K^\ell$  decreases the curves obtained from Eqs. (S6) and (S9) become more and more similar showing that the fluctuations in  $\Delta'_{c\ell}(0)$  are indeed the dominant ones.

The power-law distribution of Kondo temperatures describes only the low- $T_K$  tail of the full distribution  $P(T_K)$  and we then expect that our asymptotic expressions in Eqs. (S11) and (S12) to work better and better as  $\alpha$

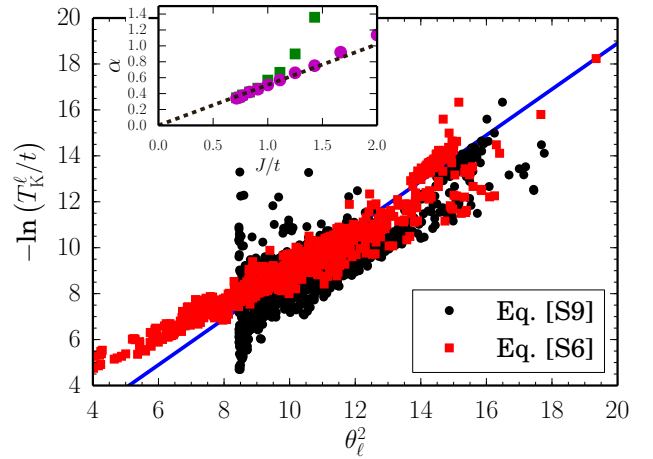


Figure S3: Octagonal tiling. Scatter plot of the numerically calculated  $-\ln(T_K^\ell)$  as a function of the exponent  $\theta_\ell^2$  with  $\theta_\ell^2 = \pi(\Delta'_{f\ell}(0) + |E_f|)/2\Delta''_{f\ell}(0)$  (Eq. (S6)) or  $\theta_\ell^2 = \pi(\Delta'_{c\ell}(0))^2/J\langle\Delta''_c(0)\rangle$  (Eq. (S9)). Each point correspond to a given site in the approximant and the straight line has a unity slope. Here, we considered the  $N_a = 1393$  approximant,  $J = 0.77t$ , and  $\mu = -2.2t$ . Inset: Power-law exponent  $\alpha$  for  $\mu = -2.2t$  as a function of the Kondo coupling  $J$ . The squares correspond to the exponent extracted from the numerical data as in Fig. 3 of the main text. The circles correspond to the exponent extracted from a distribution of  $T_K$  generated according to Eq. (S6). The dashed line is the asymptotic expression for  $\alpha$  in Eq. (S12). The error bars for  $\alpha$  are smaller than the symbol sizes.

(or  $J$ ) diminishes. To check this, we compare the exponent  $\alpha$  from our numerical data with: (i) the exponent extracted from a distribution of  $T_K$  generated according to Eq. (S6); and (ii) the asymptotic expression for  $\alpha$  in Eq. (S12). In the inset of Fig. S3 we show that all three values of  $\alpha$  nicely match for  $J \lesssim 1t$ .

#### IV. SINGULAR KONDO TEMPERATURE DISTRIBUTION AND NFL BEHAVIOR

As we discussed in the main text, the region in which  $\alpha < 1$  corresponds to NFL behavior at low- $T$ . To establish this link, we combine our  $T = 0$  solution of the mean field equations (S3) and (S4) with the well-known scaling relations for the Kondo impurity problem.<sup>14</sup> Essentially, we use the fact that the Kondo problem has a single energy scale, the Kondo temperature  $T_K$ , and that the observables can be written as universal functions of  $T/T_K$ .

For instance, for the local-moment susceptibility we have

$$\chi(T, T_K) \propto \frac{1}{T_K} f\left(\frac{T}{T_K}\right), \quad (\text{S13})$$

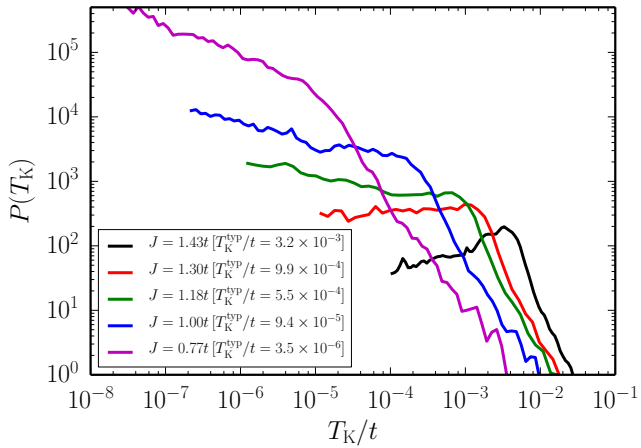


Figure S4: Octagonal tiling. Distribution of the local Kondo temperatures  $P(T_K)$  as a function of  $T_K$  on a log-log scale for several values of the Kondo coupling  $J$ .  $J$  increases from the top to the bottom curve. We see that for  $T_K \lesssim T_K^{\text{typ}}$  this distribution acquires a power-law form  $P(T_K) \sim T_K^{\alpha-1}$ . The power-law exponent  $\alpha$  continuously varies with the coupling  $J$  and for  $\alpha < 1$  we have a singular distribution (notice that for  $T_K \gtrsim T_K^{\text{typ}}$ ,  $P(T_K)$  is also power-law like, with a power that does not depend on  $J$ . This is *not* the power-law regime we refer to in this work). Here we considered  $N_a = 1393$ ,  $\mu = -2.2t$ , and  $N_\phi = 576$ .

with the asymptotic forms of  $f(x)$  given by<sup>14</sup>

$$f(x) = \begin{cases} a - bx^2 & x \ll 1 \\ (c/x)(1 - 1/\ln x) & x \gg 1 \end{cases}, \quad (\text{S14})$$

where  $a$ ,  $b$ , and  $c$  are universal numbers. The average value of the susceptibility is then given by

$$\begin{aligned} \langle \chi(T) \rangle &= \int dT_K P(T_K) \chi(T, T_K) \\ &= \chi_r + \underbrace{\int_0^{T_K^{\text{max}}} dT_K T_K^{\alpha-1} \frac{1}{T_K} f\left(\frac{T}{T_K}\right)}_{\propto T^{\alpha-1}}. \end{aligned} \quad (\text{S15})$$

Here,  $T_K^{\text{max}} \sim T_K^{\text{typ}}$  is a cutoff below which the power-law form of  $P(T_K)$  holds and we see that  $\langle \chi(T) \rangle$  contains a regular part  $\chi_r$  and a potentially singular contribution  $\chi_s \propto T^{\alpha-1}$ . For  $\alpha < 1$  and at low- $T$ , we may then disregard  $\chi_r$  to obtain the anticipated NFL power-law divergence  $\langle \chi(T) \rangle \propto T^{\alpha-1}$ . The impurity specific heat divided by the temperature has a similar behavior and, accordingly, we get  $\langle C/T \rangle \propto T^{\alpha-1}$ .

Given that the SB mean-field approach can be applied at finite- $T$  (albeit resulting in an unphysical finite-temperature transition) it is then natural to ask ourselves whether it is legitimate to calculate  $P(T_K)$  at  $T = 0$ , and follow the procedure described above, rather than solving the SB equations at finite- $T$  to explicitly calculate  $\chi(T)$  and  $\gamma(T)$ . From our experience, the general conclusion is that the leading low- $T$  power-law behavior of  $\chi$

or  $C/T$  is not affected by these additional effects. Higher- $T$  behavior will of course be affected but as long as we are interested in leading low- $T$  asymptotics (the value of the power), the current procedure is well-defined, simply because the distributions  $P(T_K)$  are very broad. Similar questions have been raised in the more general context of Quantum Griffiths Phases and the Infinite-Randomness Fixed Point Behavior.<sup>15</sup> There again one arrives at a similar conclusion: the  $T = 0$  distribution of energy dominates even finite- $T$  behavior.<sup>16-18</sup>

In the same spirit, we may extend the above discussion to also calculate observables other than thermodynamical. An interesting quantity to look at is the nuclear spin-lattice relaxation rate divided by temperature  $1/(T_1T)$ . In our Griffiths scenario, we expect that  $1/(T_1T) \sim T^{\alpha-2} \sim \chi/T$ .<sup>18-20</sup> Nevertheless, the experiment finds that  $1/(T_1T) \sim \chi$ .<sup>21</sup> We point out, however, that this discrepancy is not, at this point, particularly conclusive, since the curves for  $1/(T_1T)$  in Ref. 21 were obtained only for  $T > 1K$ , whereas the NFL behavior is more pronounced for  $T < 1K$ . It would be nice to see how  $1/(T_1T)$  behaves at low temperatures, where it will most certainly provide more conclusive hints as for the nature of quasicrystalline electronic environment. Another interesting quantity to investigate is the resistivity.<sup>19,20</sup> However, unlike thermodynamic responses, for which we expect the single impurity behavior to survive in the dense lattice limit (as is the case of  $\text{Au}_{51}\text{Al}_{34}\text{Yb}_{15}$ ), we know that for transport the situation will be different as coherence between the impurities emerges and thus we cannot, at this point, compare our predictions to the experiments. Furthermore, we expect this to be a non-trivial problem, because even in the absence of correlations, transport in quasicrystals is known to display an unusual ‘‘super-diffusive’’ behavior.<sup>5,6,22</sup>

## V. SIZE DEPENDENCE OF $P(T_K)$

In this work, we consider different values of  $N_a$  in order to establish what happens for a true quasicrystal ( $N_a \rightarrow \infty$ ). As we mention in the main text, for all approximants sizes  $N_a$  we find a minimum Kondo temperature in the sample,  $T_K^{\text{min}}$ . For the smaller approximants, the six local environments of the octagonal tiling (Fig. 1(b) of the main text) appear in a modest number of different arrangements. In other words, their extended environment, including next-nearest and further neighbors is limited. This leads not only to an appreciable  $T_K^{\text{min}}$  but also to few distinct values of  $T_K$ . As we increase the approximant size, these local environments appear in further unique configurations leading to more and more values of  $T_K$  in the sample. Therefore, we expect the statistics of  $T_K$  to improve with  $N_a$ , which can be clearly seen in Fig. S5, where, for instance, the peak around  $T_K^{\text{typ}} \sim 10^{-3}t$  (which hardly varies with  $N_a$ ) becomes ever more well defined as the system size increases. The most important, however, is the ubiquitous presence of

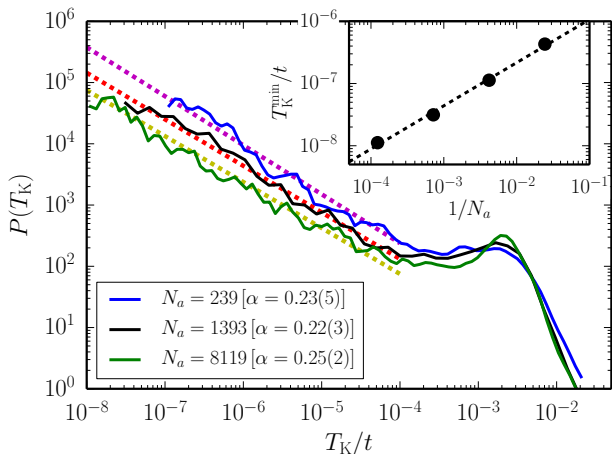


Figure S5: Octagonal tiling. Distribution of Kondo temperatures  $P(T_K^{\max})$  as a function of  $T_K$  for  $\mu = -2.0t$  and  $J = 2.0t$  and three different approximant sizes  $N_a$ . The dashed lines are a power-law fits with  $T_K^{\max} = 10^{-4}t$  with the corresponding exponents  $\alpha$  shown in the caption. Inset: Minimum value of the Kondo temperature  $T_K^{\min}$  a function of the inverse approximant size. The dashed line is a power-law fit with  $T_K^{\min} \propto N_a^{-0.69}$ .

the power-law tail at low- $T_K$  in Fig. S5 for all three approximant sizes with the same exponent (within error bars). Moreover, it is also clear from Fig. S5 that  $T_K^{\min}$  is suppressed with increasing  $N_a$ . Indeed, in the inset of Fig. S5 we find a power-law dependence of  $T_K^{\min}$  on  $N_a$ :  $T_K^{\min} \propto N_a^{-0.69}$ . Such power-law finite-size scaling (with a nontrivial power) is precisely what one expects in a critical state (in a conventional metal, for instance, one would expect power-law finite-size scaling—as it is gapless—but with integer powers).

Within our model, FL behavior is restored below  $T_K^{\min}$  as all local moments are then screened. Since the power-law distribution of Kondo temperature  $P(T_K) \propto T_K^{\alpha-1}$  emerges for  $T_K < T_K^{\text{typ}}$ , we could expect, in principle, the NFL range to be constrained to the interval  $T_K^{\min} < T < T_K^{\text{typ}}$ . However, as Fig. S5 shows,  $T_K^{\min}$  vanishes as  $N_a$  increases while  $T_K^{\text{typ}}$  remains finite. We thus conclude that the NFL range actually extends down to  $T = 0$  in a real quasicrystal. Therefore, our results suggest that it is not their local structure, but the lack of long-distance periodicity which induces robust NFL behavior in quasicrystals.

## VI. NUMERICAL CALCULATION OF THE POWER-LAW EXPONENT $\alpha$

Here we address how we calculate the power-law exponent  $\alpha$  governing the low- $T_K$  part of the distribution of Kondo temperatures. The straightforward way is to plot  $P(T_K)$  on a log-log scale and then extract  $(\alpha - 1)$  as the slope of the resulting straight line. While well defined, this procedure extracts  $\alpha$  not from the data itself, but

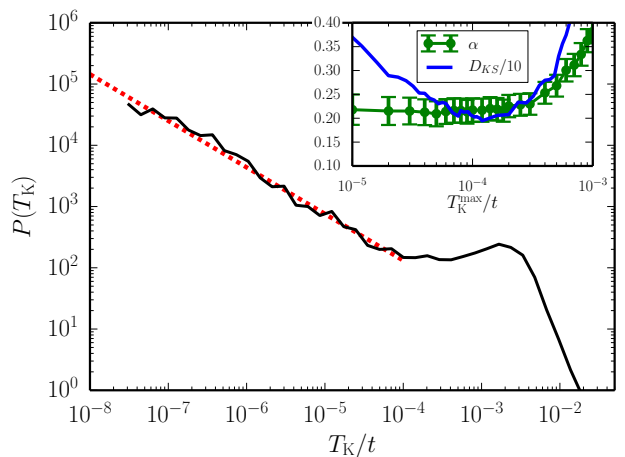


Figure S6: Octagonal tiling. Distribution of Kondo temperatures  $P(T_K)$  as a function of  $T_K$  for  $\mu = -2.0t$  and  $J = 2.0t$ . The dashed line shows a power-law fit with  $\alpha = -0.24$  and  $T_K^{\max} = 10^{-4}t$ . Inset: The circles shows the value of  $\alpha$ , as calculated from Eq. (S16), whereas the full line show the Kolmogorov-Smirnov (KS) test as a function of  $T_K^{\max}$ . Here we considered the  $N_a = 1393$  approximant.

from a given histogram. We complement the latter procedure calculating  $\alpha$  directly from the data as explained in Ref. 23.

Given a data set containing  $n$  observations  $T_K \leq T_K^{\max}$ , where  $T_K^{\max}$  is the largest value of the energy scale for which the power-law distribution holds, the value of  $\alpha$  that is most likely to have generated our data is given by

$$\alpha = \frac{n}{\sum_{i=1}^n \ln [T_K^{\max}/T_K^i]}, \quad (\text{S16})$$

with an error

$$\sigma_\alpha = \alpha/\sqrt{n}. \quad (\text{S17})$$

In practice, however, the greatest source of error comes from not choosing an optimal value for  $T_K^{\max}$ , which we dub  $T_K^{\max*}$ . We then implement two procedures to estimate  $T_K^{\max*}$ .<sup>23</sup> In the first one, we plot  $\alpha \times T_K^{\max}$  and define  $T_K^{\max*}$  as the point around which  $\alpha$  is stable as we vary  $T_K^{\max}$ . The second procedure follows the spirit of a chi-square test. The idea is to investigate how well our data is fitted by a power-law distribution. Since we are now dealing with distributions, we implement the so-called Kolmogorov-Smirnov (KS) test.<sup>11</sup> The KS statistics  $D_{KS}$  is defined as the maximum value of the absolute difference between the two *cumulative* distribution functions. We then attempt to minimize  $D_{KS}$  as a function of  $T_K^{\max}$ .

In Fig. S6 we illustrate the discussion above. In the main panel we show  $P(T_K)$  on a log-log plot accompanied by a power-law fit to its low- $T_K$  tail. In the fit displayed here, we considered  $T_K^{\max} = 10^{-4}t$  and obtained  $\alpha = 0.24$ . In the inset we then show our two proposed tests to estimate  $T_K^{\max*}$ . We see that the the  $D_{KS}$  statistics

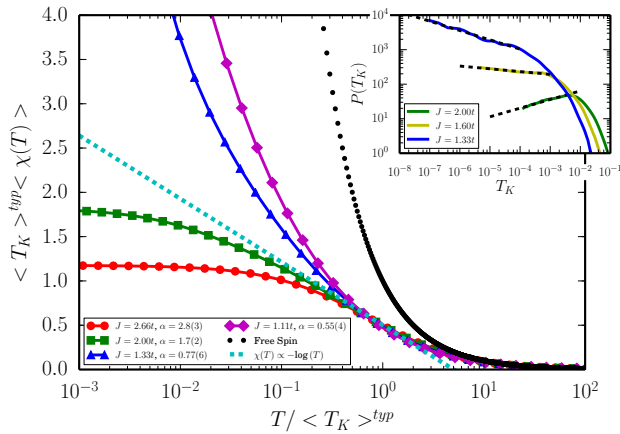


Figure S7: Icosahedral tiling. Averaged value of the impurity susceptibility  $\langle \chi(T) \rangle$  times the typical value of the Kondo temperature  $T_K^{\text{typ}}$  as a function of the temperature  $T$  normalized by  $T_K^{\text{typ}}$  for four values of the Kondo coupling  $J$  on a semi-log scale. For completeness, we show both the free spin and the  $\chi \propto -\log(T)$  ( $\alpha = 0$ ) curves. Inset: Distribution of the local Kondo temperatures  $P(T_K)$  as a function of  $T_K$  on a log-log scale for three values of the Kondo coupling  $J$ .  $J$  increases from the top to the bottom curve. At low  $T_K$  this distribution acquires a power-law form  $P(T_K) \sim T_K^{\alpha-1}$ . The power-law exponent  $\alpha$  continuously varies with the coupling  $J$  and for  $\alpha < 1$  we have a singular distribution. Here we considered  $\mu = -3.0t$ ,  $N_a = 576$ , and  $N_\phi = 512$ .

has a minimum around  $T_K^{\text{max}} = 10^{-4}t$  and that in this region  $\alpha$  is essentially flat as a function of  $T_K^{\text{max}}$ , with a value of  $\alpha = 0.22 \pm 0.03$ .

## VII. DIFFERENT TILINGS

So far we have investigated the single-impurity Kondo effect in the octagonal tiling, a  $2D$  quasicrystal, while the original motivation came from experiments on a  $3D$  heavy fermion quasicrystal  $\text{Au}_{51}\text{Al}_{34}\text{Yb}_{15}$ ,<sup>21,24</sup>. In the following we show that this difference in spatial dimensionality does not change the qualitative behavior of

Kondo impurities. First we note that the importance of spatial dimensionality in determining the statistics of wavefunction amplitudes (e.g. the local density of states statistics) is well known in disordered systems.<sup>25</sup> For this problem,  $2D$  and  $3D$  are significantly different because  $2D$  is the lower critical dimension for Anderson localization.<sup>26</sup> Second, however, it is known that some models for low-dimensional (even  $1D$ ) quasicrystals can support extended or pseudo-extended electronic states, and even a sharp Anderson-like transition and a mobility edge.<sup>27</sup> In this sense,  $2D$  is most likely *not* the lower critical dimension for wavefunction localization in quasicrystals. Hence, there should not be a significant qualitative difference between electronic quasicrystalline states in  $2D$  and  $3D$ .<sup>6</sup> Therefore we expect that our  $2D$  results capture the key effects of the quasicrystalline wavefunctions on the Kondo effect in general, and that our conclusions should remain valid in  $3D$  thus providing a robust and general scenario for the emergence of NFL behavior in quasicrystals.

To support the claim that our results are general and applicable to different tilings (even to  $3D$  quasicrystals), we have studied the Kondo problem in the  $3D$  icosahedral tiling.<sup>28</sup> This tiling possesses 7 distinct local environments with coordination number  $z = 4, \dots, 9$ , and 12. The average coordination number is 6 and the bandwidth is comparable to that of the simple cubic lattice. Sample results are presented in Fig. S7. As in the octagonal tiling, we obtain a power-law distribution of Kondo temperatures,  $P(T_K) \sim T_K^{\alpha-1}$ , and the corresponding NFL behavior for  $\alpha < 1$ . As discussed in the main text, the essential ingredient for this behavior is the unanticipated Gaussian form of the local  $c$ -electron cavity function fluctuations at the Fermi level,  $\delta\Delta'_c$ , and not any special lattice symmetry or dimension.

In conclusion, the striking similarity of our results for the octagonal and icosahedral tilings shows that NFL behavior from dilute Kondo impurities in quasicrystals is robust and serves as a starting point to understand quasicrystalline Kondo lattices, in order to connect to the recently observed NFL behavior in the  $3D$  heavy fermion quasicrystal  $\text{Au}_{51}\text{Al}_{34}\text{Yb}_{15}$ .<sup>21,24</sup>

<sup>1</sup> M. Kohmoto, B. Sutherland, and C. Tang, Phys. Rev. B **35**, 1020 (1987).

<sup>2</sup> A. Chhabra and R. V. Jensen, Phys. Rev. Lett. **62**, 1327 (1989).

<sup>3</sup> A. Richardella, P. Roushan, S. Mack, B. Zhou, D. A. Huse, D. D. Awschalom, and A. Yazdani, Science **327**, 665 (2010).

<sup>4</sup> A. Rodriguez, L. J. Vasquez, K. Slevin, and R. A. Römer, Phys. Rev. Lett. **105**, 046403 (2010).

<sup>5</sup> A. Jagannathan and F. Piéchon, Philos. Mag. **87**, 2389 (2007).

<sup>6</sup> U. Grimm and M. Schreiber, in *Quasicrystals - Structure and Physical Properties*, edited by H.-R. Trebin (Wiley-

VCH, Weinheim, 2003), pp. 210–235.

<sup>7</sup> A. D. Mirlin, Phys. Rep. **326**, 259 (2000).

<sup>8</sup> G. Schubert, J. Schleede, K. Byczuk, H. Fehske, and D. Vollhardt, Phys. Rev. B **81**, 155106 (2010).

<sup>9</sup> C. Gros, Phys. Rev. B **53**, 6865 (1996).

<sup>10</sup> F. F. Assaad, in *Quantum Simulations of Complex Many-Body Systems: From Theory to Algorithms*, edited by J. Grotendorst, D. Marx, and A. Muramatsu ((John von Neumann Institute for Computing (NIC), 2002).

<sup>11</sup> William H. Press *et al.*, *Numerical Recipes: The Art of Scientific Computing* (Cambridge University Press, 2007), 3rd ed.

<sup>12</sup> D. Tanasković, E. Miranda, and V. Dobrosavljević, Phys.

- Rev. B **70**, 205108 (2004).
- <sup>13</sup> A. Jagannathan, Phys. Rev. B **61**, R834 (2000).
- <sup>14</sup> A. C. Hewson, *The Kondo Problem to Heavy Fermions* (Cambridge University Press, Cambridge, 1993), 1st ed.
- <sup>15</sup> D. S. Fisher, Phys. Rev. B **51**, 6411 (1995).
- <sup>16</sup> E. Miranda and V. Dobrosavljević, Rep. Prog. Phys. **68**, 2337 (2005).
- <sup>17</sup> T. Vojta, J. Phys. A: Math. Gen. **39**, R143 (2006).
- <sup>18</sup> T. Vojta, J. Low Temp. Phys. **161**, 299 (2010).
- <sup>19</sup> E. Miranda, V. Dobrosavljević, and G. Kotliar, J. Phys. Cond. Mat **8**, 9871 (1996).
- <sup>20</sup> E. Miranda, V. Dobrosavljević, and G. Kotliar, Phys. Rev. Lett. **78**, 290 (1997).
- <sup>21</sup> K. Deguchi, S. Matsukawa, N. K. Sato, T. Hattori, K. Ishida, H. Takakura, and T. Ishimasa, Nat. Mater. **11**, 1013 (2012).
- <sup>22</sup> H. Q. Yuan, U. Grimm, P. Repetowicz, and M. Schreiber, Phys. Rev. B **62**, 15569 (2000).
- <sup>23</sup> A. Clauset, C. R. Shalizi, and M. E. J. Newman, SIAM Review **51**, 661 (2009).
- <sup>24</sup> T. Watanuki, S. Kashimoto, D. Kawana, T. Yamazaki, A. Machida, Y. Tanaka, and T. J. Sato, Phys. Rev. B **86**, 094201 (2012).
- <sup>25</sup> P. W. Anderson, Phys. Rev. **109**, 1492 (1958).
- <sup>26</sup> E. Abrahams, P. W. Anderson, D. C. Licciardello, and T. V. Ramakrishnan, Phys. Rev. Lett. **42**, 673 (1979).
- <sup>27</sup> J. Luck and D. Petritis, J. Stat. Phys. **42**, 289 (1986).
- <sup>28</sup> E. S. Zijlstra and T. Janssen, Europhys. Lett. **52**, 578 (2000).